Supplement of
The effect of debris-flow sediment grain size distribution on fan forming processes

Haruka Tsunetaka[1], Norifumi Hotta[2], Yuichi Sakai[3], Thad Wasklewicz[4]

[1]Forestry and Forest Products Research Institute, Ibaraki, Japan
[2]Graduate School of Agricultural and Life Sciences, The University of Tokyo, Tokyo, Japan
[3]Division of Earth and Planetary Sciences, Graduate School of Science, Kyoto University, Kyoto, Japan
[4]Stantec Inc, Environmental Services, Geohazards and Geomorphology Group, Fort Collins, CO, USA

Correspondence to: Haruka Tsunetaka (tsunetakaharuka@ffpri.affrc.go.jp)

Section S1 Equipment Specification.

Ultrasonic sensor

Model: Omron E4PA

Sampling frequency: 50 Hz

Note: The ultrasonic sensors measured the flow or initial bed surface at a point scale. The measurements are susceptible to local undulations in the flow surface and erodible bed. Accordingly, some spikes of the flow surface ranging from approximately 0.03 to 0.05 m were measured especially for the middle and lower locations, but these impacts were ephemeral (Fig. 2).

Erodible bed saturation was not completely controlled because it included voids. Saturated bed conditions were approximated by carefully supplying clear water across the entire erodible bed using watering cans just before we started the water supply from the upper end of the flume. However, by suppling this water before the debris flow was generated, we may have inadvertently caused the initial bed surface to undulate, as the water level may have increased at some places in the erodible bed and the bed surface may have been disturbed. Indeed, measurements from the displacement meter set in the middle location of the flume indicated that there was a local undulation of approximately 3 cm in multi-granular run 2 (Fig. 2E). However, following the descent of the flow front, the hydrographs for all the tests were similar, irrespective of measurement positions (Fig. 2), which suggests that any impact from local undulations in the initial bed surface were canceled by the steady entrainment of channel sediment as the flow descended.

Digital single-lens reflex cameras for SfM-MVS

Model: Nikon D5100

Sensor size: 23.6 × 15.6 mm

Image size: 4928 × 3264 pixels

Pixel size: 4.78 μm

Release shutter of the digital cameras for SfM-MVS

Model: Canon TC-80N3

Shutter interval: 1 s

Digital single-lens reflex camera for PIV (recording video)

Model: PENTAX K-3 II

Sensor size: 23.6 × 15.6 mm

Image size: 1920 × 1080 pixels

Frame rate: 60 fps

Pixel size: 14.44 μm

Section S2 Software Specification.

Software for SfM-MVS

Software: Agisoft Metashape Professional 1.5.1

DEM resolution: 1 mm

Orthophoto resolution: 1 mm

Software for PIV

Software: Image J

Plugin for analysis: PIV (Particle Image Velocimetry) developed by Tseng et al. (2012).

Using algorism: cross-correlation algorism

References: Tseng, Q., Duchemin-Pelletier, E., Deshiere, A., Balland, M., Guillou, H., Filhol, O., and Théry, M., 2012, Spatial organization of the extracellular matrix regulates cell-cell junction positioning: Proceedings of the National Academy of Sciences of the United States of America, v. 109, p. 1506–1511.

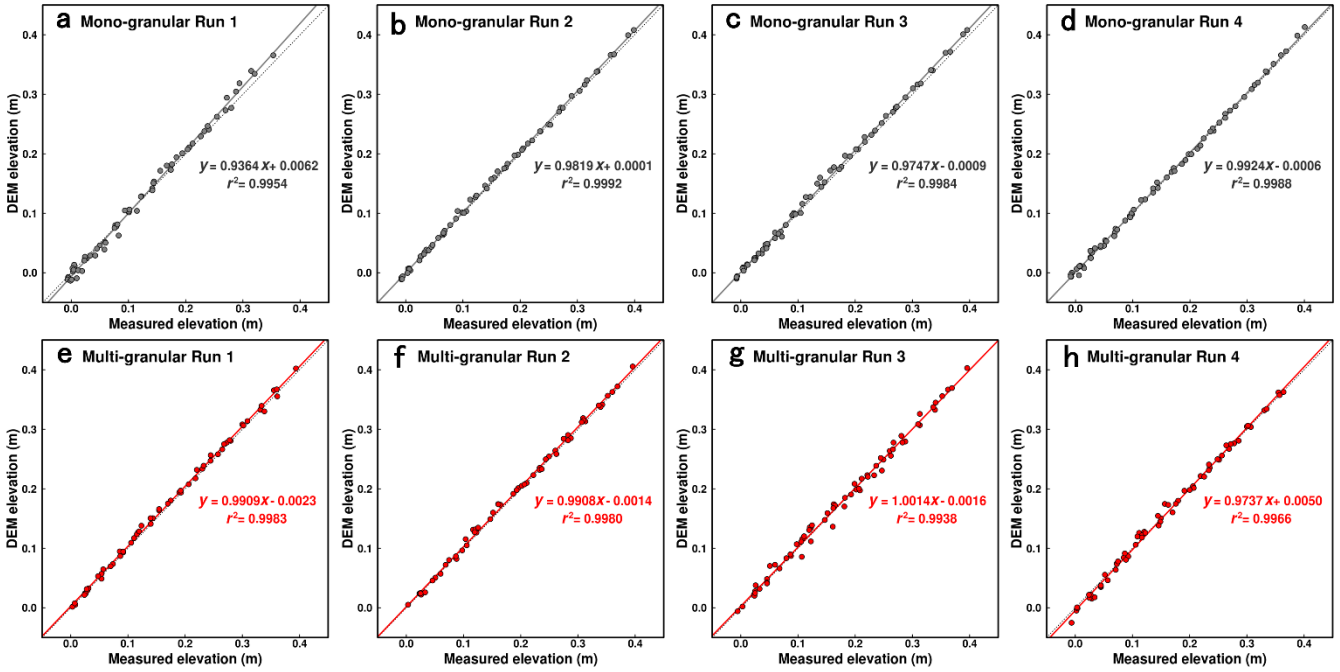

Figure S1: Final topographies of the debris-flow fans. (a–d) mono-granular flows. (e–h) multi-granular flows. The elevation is depicted assuming that the area with a 3° slope (i.e., the area further downstream from the point where the slope changed from 3° to 6°) has an elevation of zero.

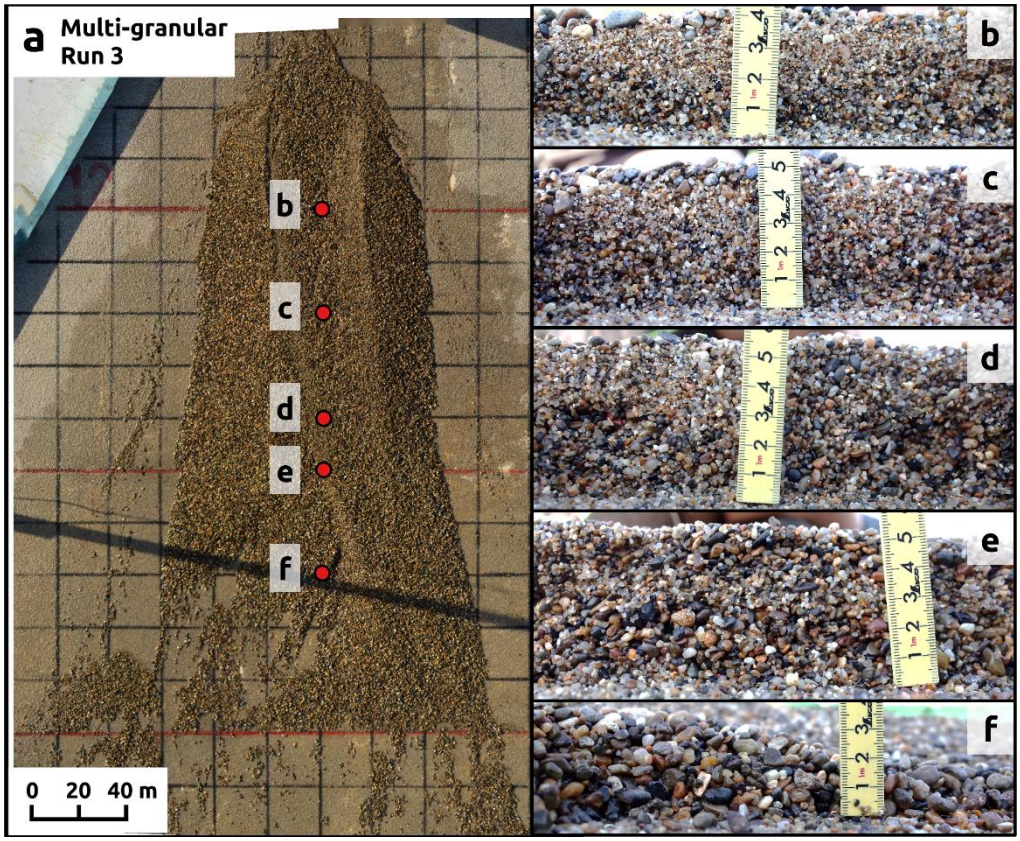

Figure S2: (a) Orthophoto for the debris-flow fan that formed from the multi-granular flow (run 3). The red points indicate the points where the images were taken. (b) image of the longitudinal profile 1 m downstream from the flume outlet (change point of the slope from 12° to 9°). (c) image of the longitudinal profile 1.4 m downstream from the flume outlet. (d) image of the longitudinal profile 1.8 m downstream from the flume outlet. (e) image of the longitudinal profile 2 m downstream from the flume outlet (change point of the slope from 9° to 6°). (f) image of the longitudinal profile 2.4 m downstream from the flume outlet.

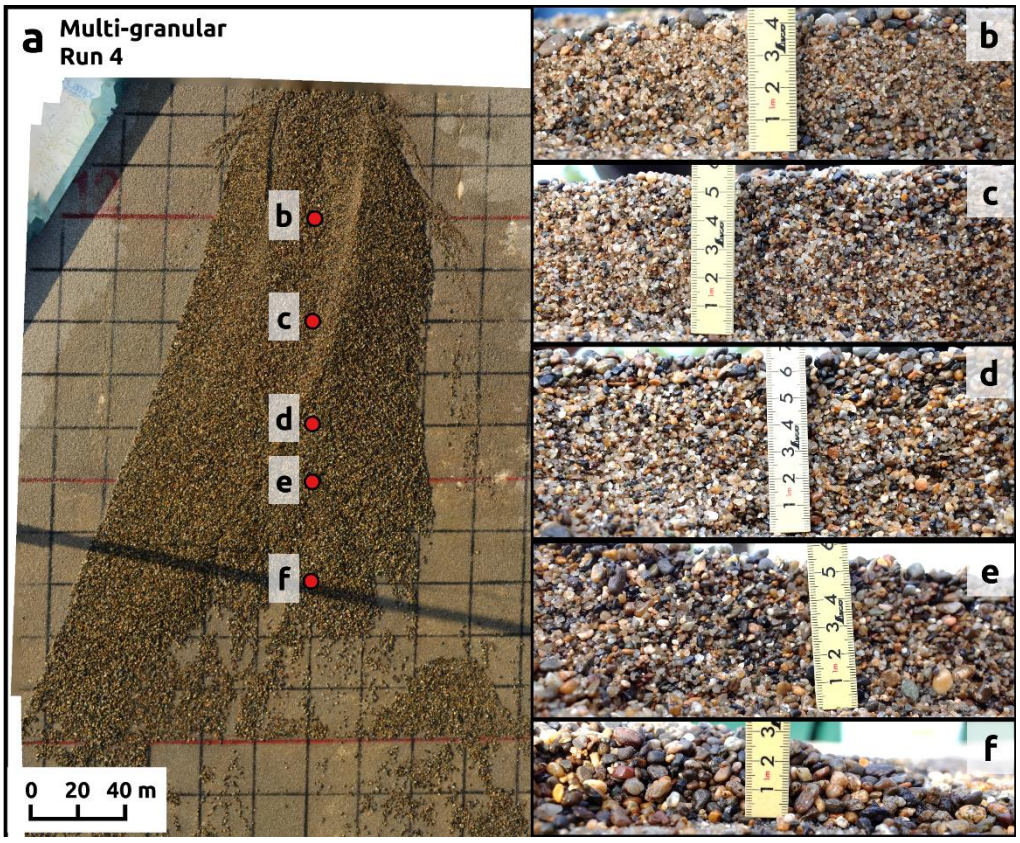

Figure S3: (a) Orthophoto for the debris-flow fan that formed from a multi-granular flow (run 4). The red points indicate where the images were taken. (b) image of the longitudinal profile 1 m downstream from the flume outlet (slope change point from 12° to 9°). (c) image of the longitudinal profile 1.4 m downstream from the flume outlet. (d) image of the longitudinal profile 1.8 m downstream from the flume outlet. (e) image of the longitudinal profile 2 m downstream from the flume outlet (slope change point from 9° to 6°). (f) image of the longitudinal profile 2.4 m downstream from the flume outlet.

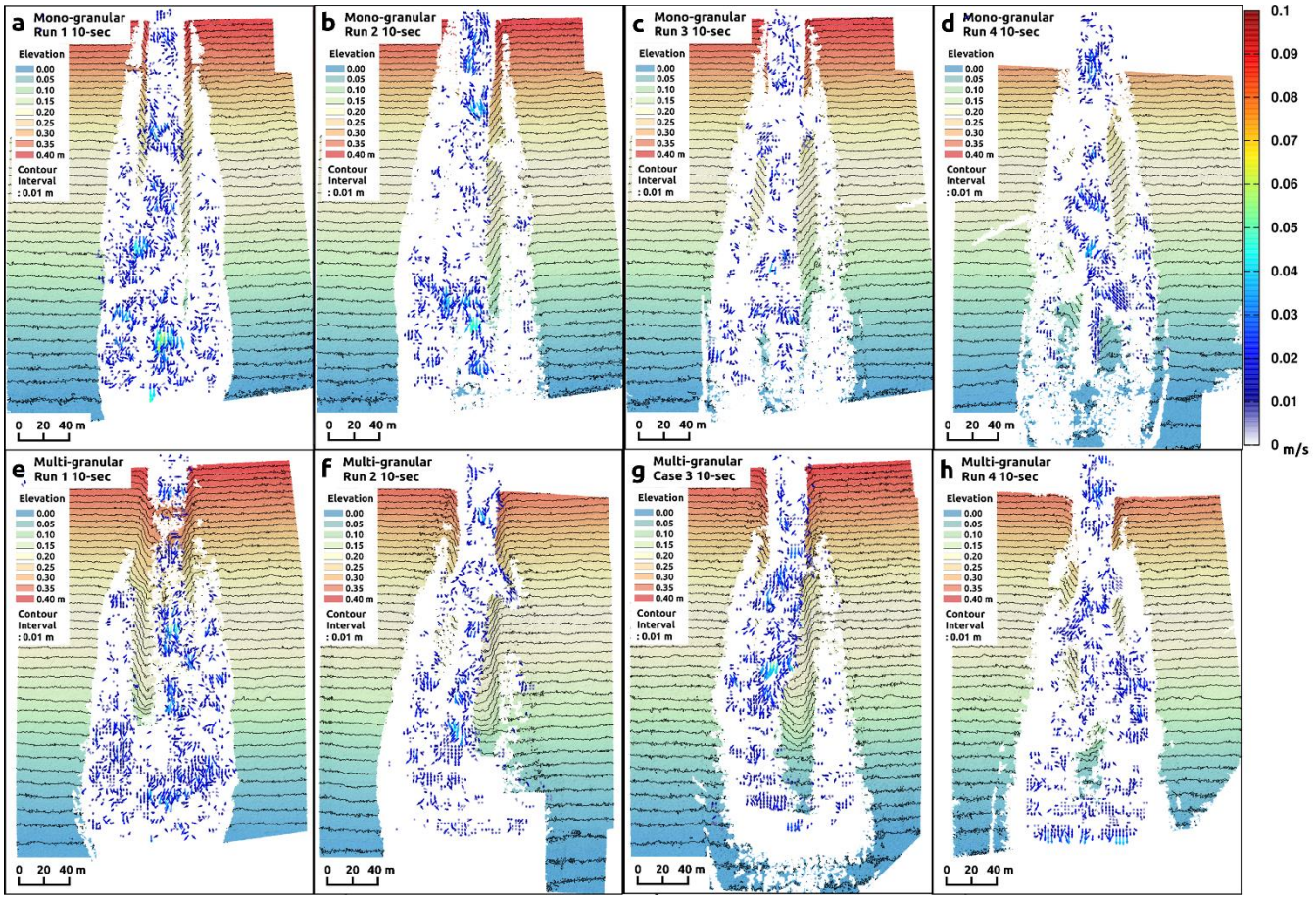

Figure S4: Fan formation and distribution of the flow vectors 10 seconds after the start of the runout. (a–d) Mono-granular flows. (e–h) Multi-granular flows. The elevation is depicted assuming that the area with a 3° slope (i.e., the area further downstream from the point the slope angle changed from 3° to 6°) has an elevation of zero.

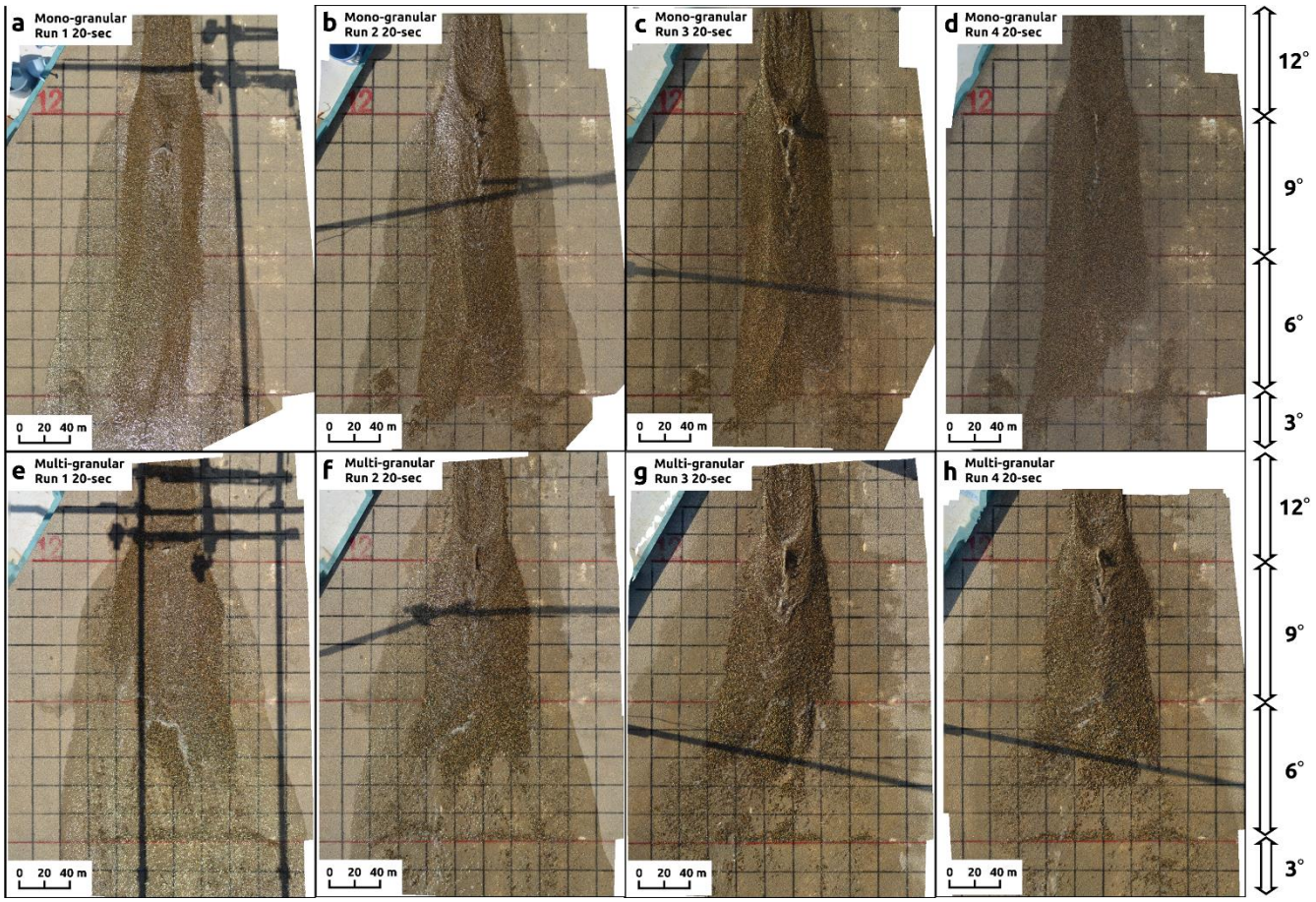

Figure S5: Orthophotos 20 seconds after the start of the runout. (a–d) Mono-granular flows. (e–h) Multi-granular flows.

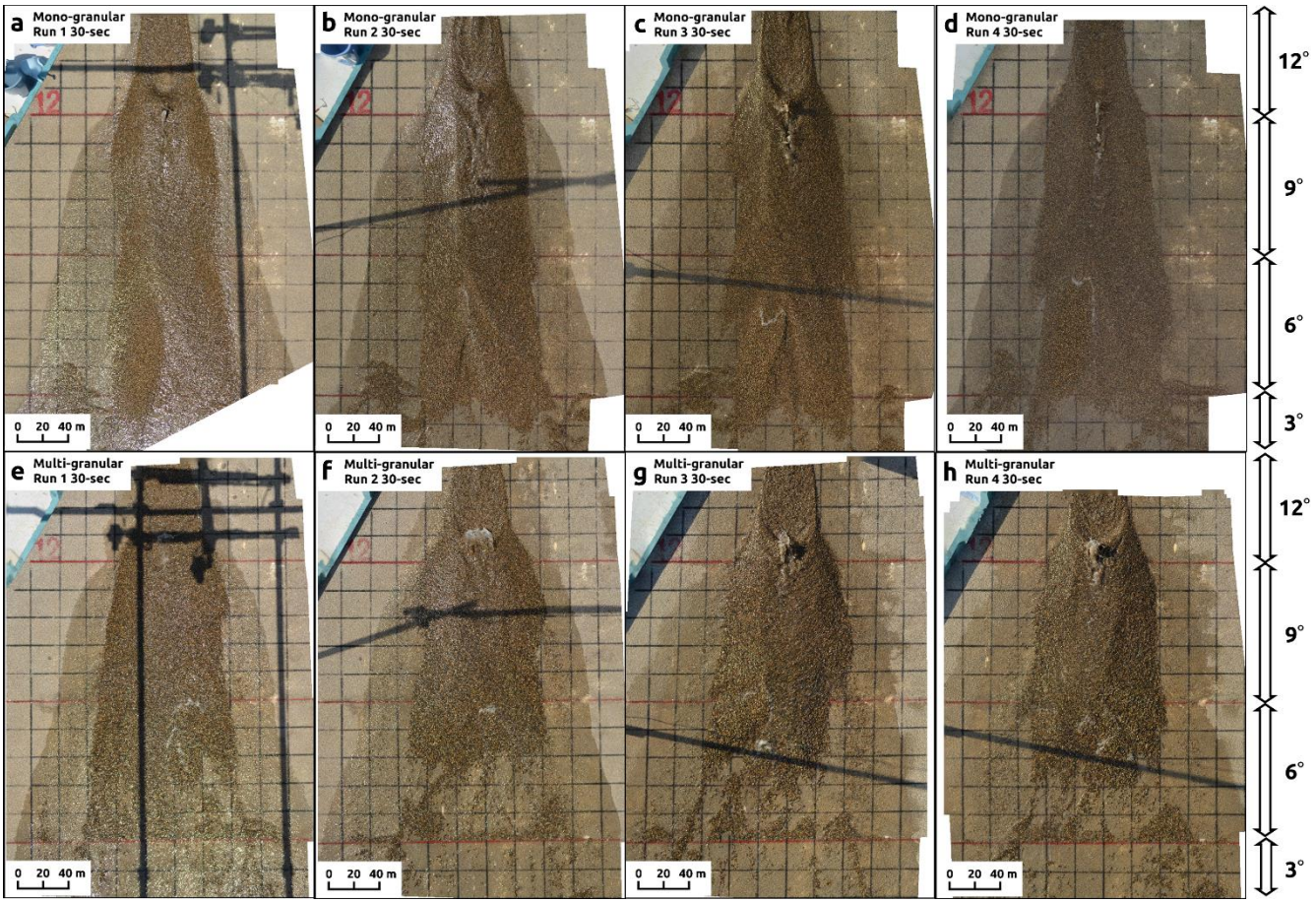

Figure S6: Orthophoto 30 seconds after the start of runout. (a–d) Mono-granular flows. (e–h) Multi-granular flows.

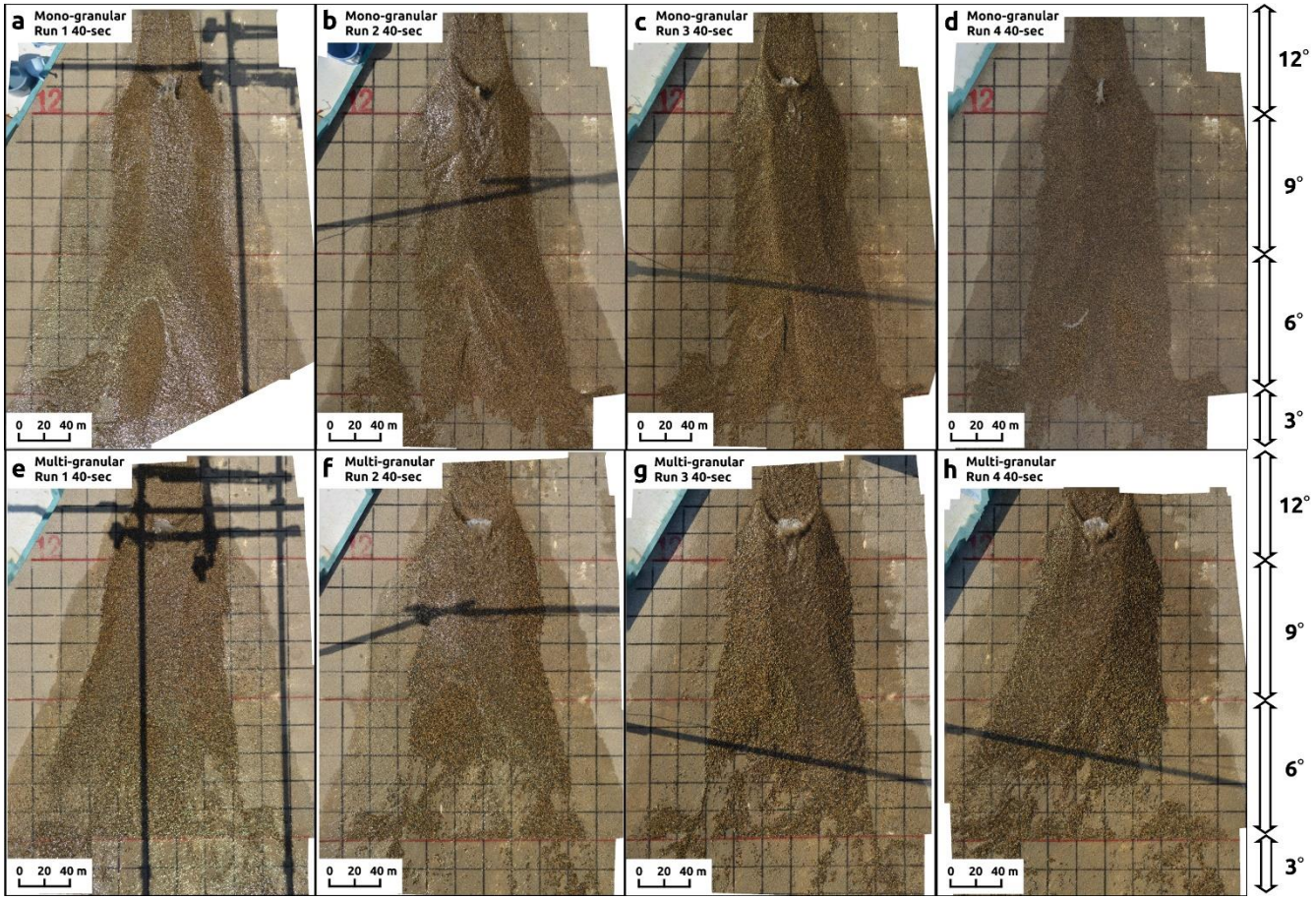

Figure S7: Orthophoto 40 seconds after the start of the runout. (a–d) Mono-granular flows. (e–h) Multi-granular flows.

90

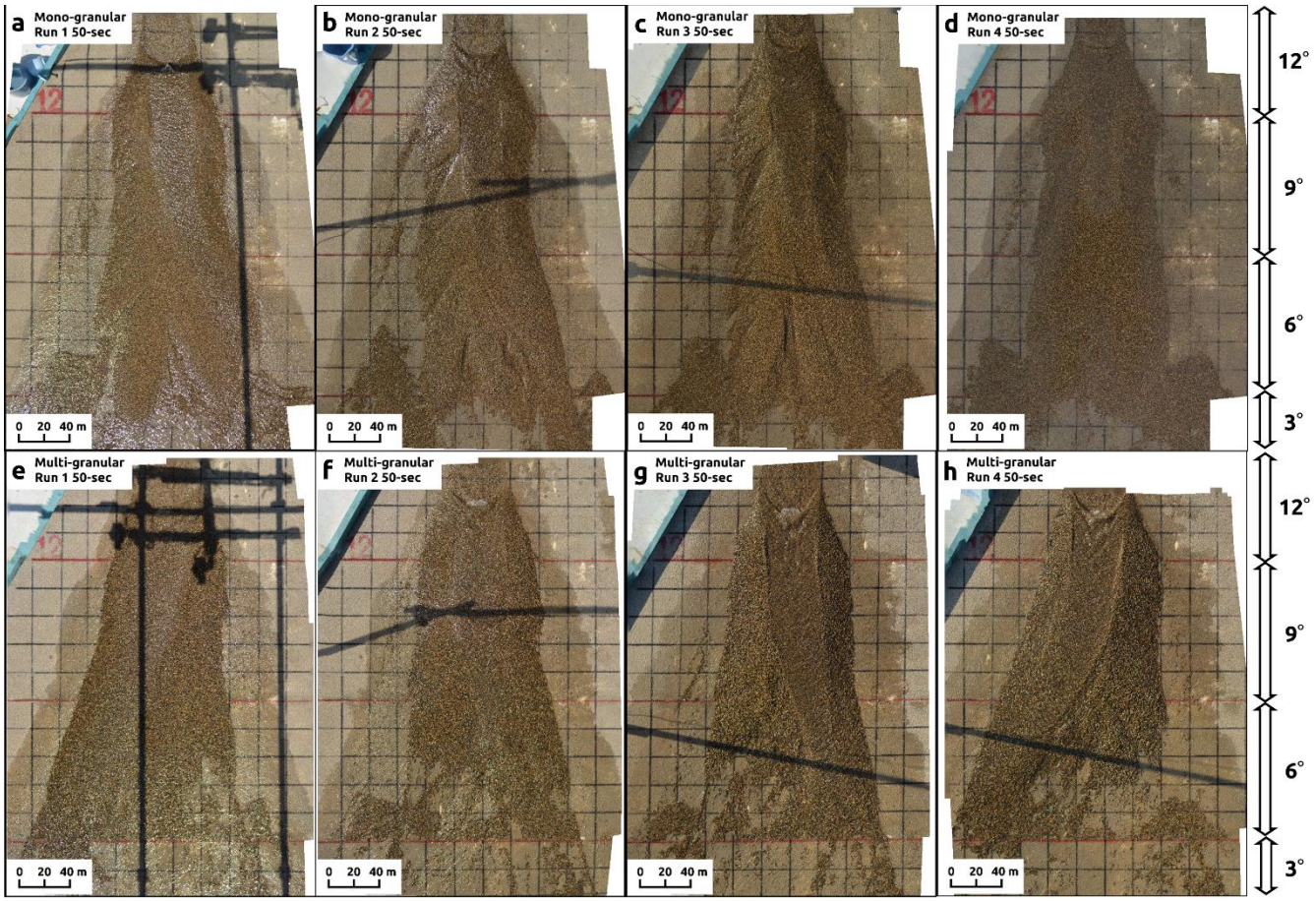

Figure S8: Orthophoto 50 seconds after the start of the runout. (a–d) Mono-granular flows. (e–h) Multi-granular flows.

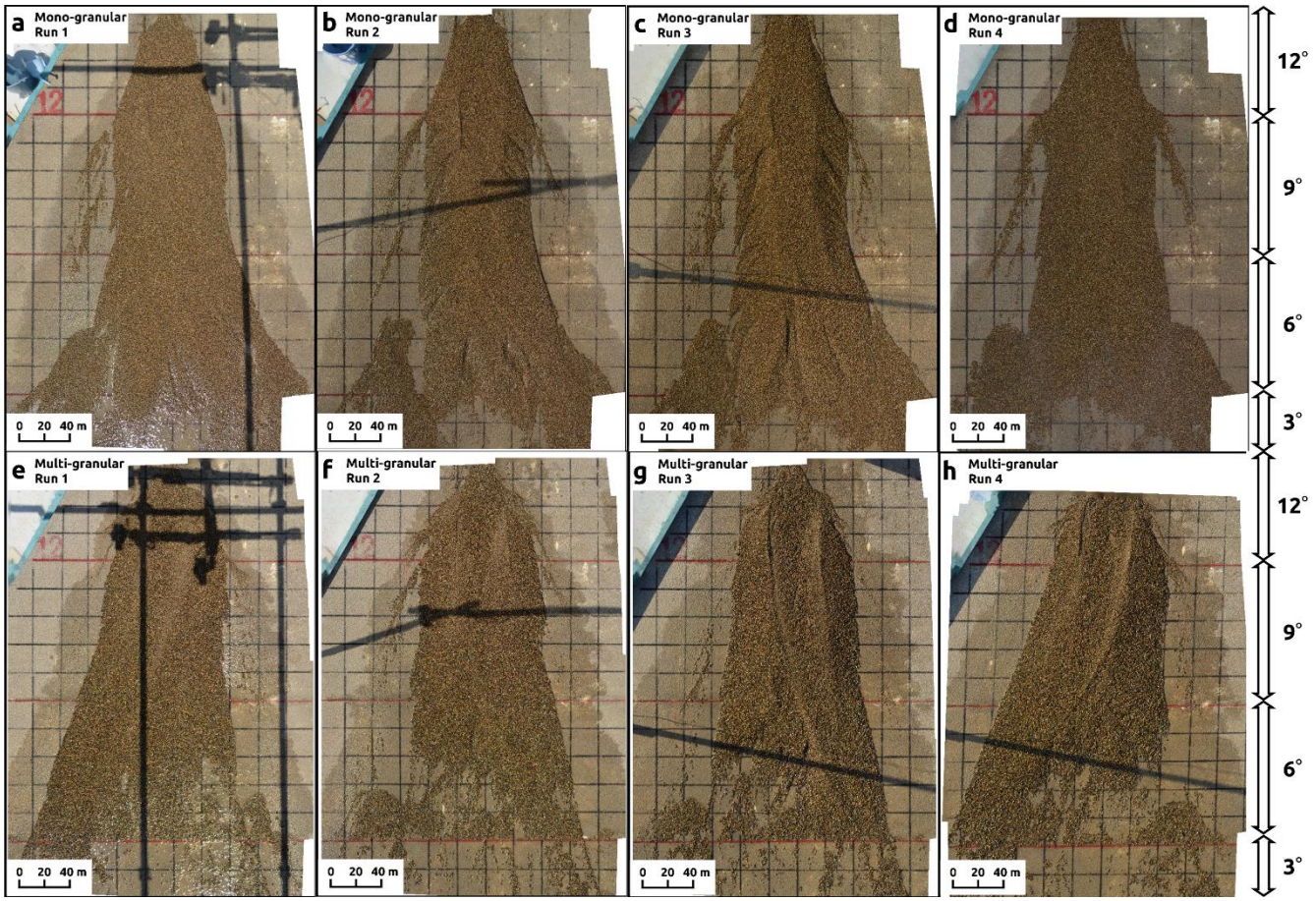

Figure S9: Orthophotos for the final fan morphology. (a–d) Mono-granular flows. (e–h) Multi-granular flows. The fans that developed from the multi-granular flows were elongated to the right bank side (in runs 1 and 4; panels e and h) or the left bank side (in runs 2 and 3; panels f and g).